Stochastic stress analysis and failure onset of variable angle tow laminates affected by spatial fibre variations

Composites Part C: Open Access 4 (2021) 100091

Contents lists available at ScienceDirect

Composites Part C: Open Access

journal homepage: www.elsevier.com/locate/jcomc

Stochastic stress analysis and failure onset of variable angle tow laminates affected by spatial fibre variations

A. Pagani*, A.R. Sanchez-Majano

MUL2 Team, Department of Mechanical and Aerospace Engineering, Politecnico di Torino Corso Duca degli Abruzzi 24, 10129 Torino, Italy

ARTICLE INFO

Keywords:
Variable angle tow composites
Defect modelling
Uncertainty analysis
Carrera unified formulation

ABSTRACT

The usage of printed composites in the aerospace industry has been steadily increasing over the last years. Especially, 3D printers and automatic fibre placement machines have allowed the introduction of Variable Angle Tow (VAT) composites, which theoretically offer greater tailoring capabilities than classic composite laminates. Nevertheless, the steering of brittle fibres is not flaw-exempt and, in fact, is greatly affected by the printer signature. This manuscript aims to examine the influence of fibre misalignments on the stress and failure index distribution in laminated VAT composites. For doing so, the Carrera Unified Formulation (CUF) is employed to develop layerwise models with unprecedented accuracy. Flaws are introduced at the layer scale by means of stochastic fields and uncertainty analysis is carried out through a Monte Carlo analysis. The random variation (defects) is propagated through the scales and correlated with the stress and failure index distribution. The results show that misalignments greatly affect the in-plane normal stresses, which lately influence fibre tension and compression failure mechanisms.

1. Introduction

The irruption of additive manufacturing techniques such as Automatic Fibre Placement (AFP) has allowed the capability of crafting composite structures with unachievable performances if compared to those structures resulting from classic manufacturing methods. Composites coming from AFP processes can be, eventually, devised to have curved fibre paths within each lamina. These special laminates are known to as Variable Angle Tow (VAT) composites and were first analysed by Gurdal and Olmedo [1,2] in the early 90s. These seminal works showed that VAT outperform classical straight-fibre laminates in terms of redistributing stress and stiffness within the laminate, thus providing a flexibility to the designer for trade-off between overall panel stiffness and buckling load, even without increasing the size or weight of the panel as in classical straight fibre configurations may occur.

These studies, albeit a breakthrough in VAT plates, did not consider, for instance, the minimum turning radius of the AFP machine as a manufacturing constraint. Such restrictions during manufacturing lead to imperfections that subsequently affect the structural performance. A thorough review about manufacturing-induced imperfections was made by Heinecke and Willberg [3], where several methodologies for evaluating the effects of such manufacturing defects are listed, especially emphasising on gaps and overlaps. Many manuscripts regarding these latter imperfections have been written. For instance, Blom *et al.* [4] studied how tow-drop areas influence the stress and stiffness of VAT plates. In order to model the gap areas, a very refined mesh to capture such regions was needed, thus increasing the required computational effort. A non-intrusive, in terms of mesh modification, strategy for accounting these imperfections was proposed by Fayazbakhsh et al. [5] with the name of Defect Layer Method (DLM). DLM is based on subroutines that beforehand compute the gap percentage involved in a mesh element and based on that percentage, the material mechanical properties of such element are modified. Contrarily, in the case of overlap-modified the thickness increases proportionally with the overlap area percentage. By using DLM, accurate results can be obtained without the usage of a really refined mesh. As demonstrated in the aforementioned works, flaws affect the performance of the structure and, therefore, have to be considered during the optimisation process as well, since they may lead to different optimal values of the design variables. Nik et al. [6] demonstrated that a full-overlap strategy outperforms a full-gap strategy in terms of buckling load and in-plane stiffness when compared to the defect-free structure.

Despite the efforts made to characterise the influence of such flaws, many other defects have not attracted the attention of researchers. Some of them are the angle deviation and tow misalignments. The former occur since the planning software for fibre deposition usually considers reference curves to define individual fibre courses. Those guiding curves tend to correspond to the centre line of individual fibre courses [7] and several adjacent fibres are oriented to one reference curve. When a curved fibre course is considered, a continuous deviation from the de-

* Corresponding author.
E-mail address: alfonso.pagani@polito.it (A. Pagani).

https://doi.org/10.1016/j.jcomc.2020.100091
Received 16 October 2020; Received in revised form 9 December 2020; Accepted 14 December 2020

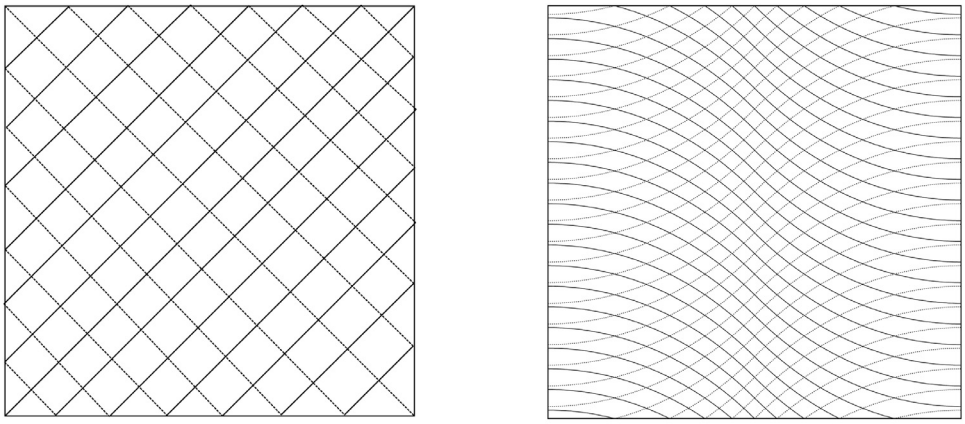

(a) $[\pm 45^{\circ}]$ straight-fibre laminate

(b) $[\pm < T_0, T_1 >]$ VAT laminate

Fig. 1. Comparison of layup sequences between classical straight-fibre and VAT laminates.

sired fibre angle (defined by the respective reference curve) over the fibre course takes place. Indeed, the wider the fibre course the larger angle variations at the course ends [6]. Therefore, a problem arises when trying to find a trade-off between deposition rate and layup quality. On the other hand, fibre misalignments are mainly due to the kinematic characteristics of the AFP machine and its control [8,9]. These two types of flaws are considered primary imperfections and lead to the aforementioned gaps and overlaps [9].

Misalignment sensitivity analysis might have not been exhaustively carried out in the case of VAT structures, but have been taken into account in classic straight-fibre laminates studies [10–13]. In fact, analytical and numerical formulations have been derived to compute the sensitiveness and response derivatives with regard to mechanical and geometrical properties. For instance, Mateus et al. [14] computed derivatives of the strain energy and natural frequencies with regard to fibre angle orientations and ply thicknesses for optimisation purposes, therefore computing such sensitivities in the considered design space. Other studies perform sensitivity analysis starting from a fixed configuration, that is, predefined fibre angle orientations, ply thicknesses and mechanical properties, and sensitivity indices are computed in order to calculate the influence of the design properties with regard to the desired magnitude. A sort of such indices are known as Sobol indices [15], which have been employed in a plethora of works [16–18]. Nonetheless, those analysis tend to assign homogeneous properties within the ply. During the last years, studies concerning the spatial variation of material properties have been carried out by Scarth et al. [19] and van den Broek et al. [20,21] in which they analysed how material and geometric variations, introduced in the structural models by means of stochastic fields, affect free vibration and buckling performance of aerospace structures. Moreover, by following a similar methodology, Pagani and Sanchez-Majano [22] were able to characterise the buckling performance of VAT plates when manufacturing flaws, such as fibre misalignments, are considered.

In this work, the Carrera Unified Formulation (CUF) is employed to model VAT plates due to its capabilities to create structural models with different accuracy levels, as demonstrated in the works by Carrera [23] and Carrera et al. [24]. In recent years, CUF was already used to analyse the behaviour of VAT laminates. A first approach was carried out by Vescovini and Dozio [25] and Vescovini et al. [26], where CUF and Ritz method were combined for the vibration and buckling analysis and to analyse the post-buckling behaviour of VAT plates respectively. Next, Demasi et al. [27,28], for instance, used zig-zag, equivalent single layer (ESL) and layerwise (LW) theories to model the through-the-thickness discretization of the displacement variables to carry out static analysis and proved the versatility of CUF against commercial software. Additionally, Viglietti et al. [29,30] carried out free vibration analyses of VAT panels using 1D models in which the cross-section behaviour was described employing ESL and LW expansions. These articles showed that LW formulations, in comparison with 3D models, represented a strong reduction of the computational cost in terms of the number of degrees of freedom and provided the most accurate solutions. LW models have the advantage of being capable of modelling the mesoscale behaviour of composite laminates, therefore manufacturing flaws such as printing defects can be considered. Following these conclusions, the proposed research aims to demonstrate that fibre misalignment may seriously affect the static failure behaviour of VAT plates. For doing so, we couple CUF-based models with stochastic fields that spatially vary the local fibre orientation. Hence, a linear static analysis is performed and stresses are computed consequently to evaluate 3D failure indices at the layer level.

The manuscript is organised as follows: Section 2 describes the constitutive behaviour of VAT composite laminates. Then, Section 3 continues by describing the mathematical treatment of stochastic fields employed for the generation of fibre misalignment. Next, Section 4 introduces the failure indices employed in this work. In Section 5, CUF-based on LW strategy are discussed along with an opportune finite element solution. Afterwards, Section 6 shows the results of the performed simulations along with the statistical treatment of stress and failure indices distribution. Finally, conclusions are drawn in Section 7.

2. Variable stiffness composites

Contrarily to straight-fibre composites, which have been extensively used throughout the years in the aerospace industry and provide a constant in-plane stiffness per lamina, in VAT plates the fibres are steered along a curvilinear path within each ply, as shown in Fig. 1. Current manufacturing processes allow to obtain a wide variety of VAT structures, from the earliest linear variation concept proposed by Gurdal [1] up to the non-linear variation of the fibre orientation showed in [31]. Both concepts are represented in Fig. 2. With no loss of generality, in this work a linear variation based on Eq. (1) is used,

$$\theta(x, y) = T_0 + \frac{(T_1 - T_0)}{d}|x| \tag{1}$$

where T_0 and T_1 are, respectively, the fibre orientation at the centre of the plate and at the plate coordinate such that $|x| = d$. Both angles are measured with regard to the x-axis. The notation used in this manuscript to represent the fibre orientation is $< T_0^k, T_1^k >$, where the apex k indicates the number of the layer. Additionally, in this manuscript, distance d corresponds to the semi-length along the x-direction of the plate, but can vary whether the fibre orientation is measured with regard to the x or y-axis.

The three-dimensional behaviour of a composite lamina made of linear elastic material can be expressed, independently of the fibre orientation angle, by means of the generalised Hooke law, which reads in the

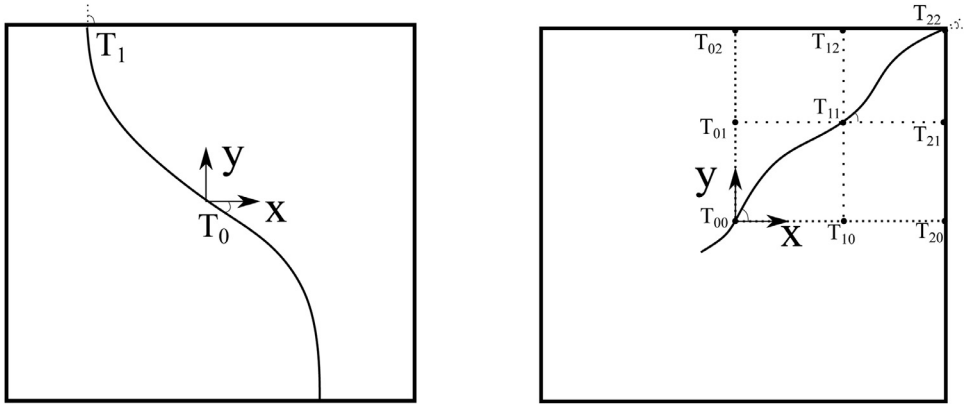

(a) Linear VAT laminate

(b) Non linear VAT laminate

Fig. 2. Notation adopted for linear and nonlinear VAT configurations.

material reference system as:

$$\boldsymbol{\sigma} = \mathbf{C}\boldsymbol{\epsilon} \tag{2}$$

in which $\boldsymbol{\sigma}$ and $\boldsymbol{\epsilon}$ correspond to the stress and strain tensors expressed in the Voigt notation, and $\mathbf{C}$ is the material stiffness matrix, which is symmetric and contains nine independent terms since the considered material in this manuscript is orthotropic. In VAT plies, the fibre orientation angle depends on the plane coordinates, i.e. $\theta(x, y)$. Thereby, the Hooke law expressed in a generic Cartesian reference frame reads as:

$$\boldsymbol{\sigma} = \widetilde{\mathbf{C}}(x, y)\boldsymbol{\epsilon} \tag{3}$$

where

$$\widetilde{\mathbf{C}}(x, y) = \mathbf{T}(x, y)\mathbf{C}(\mathbf{T}(x, y))^T \tag{4}$$

in which superscript T means transposition and $\mathbf{T}$ is the rotation matrix. Beware that matrices $\mathbf{T}$ and $\widetilde{\mathbf{C}}$ for VATs vary point-wise depending on the local fibre orientation, whereas in the case of classic laminates they remain constant within the lamina. Matrix $\mathbf{T}$ is not included in here for the sake of brevity, but the reader can find it in many reference texts, see for instance [32].

3. Random fields of fibre misalignments

In the present work, fibre misalignments due to the manufacturing processes are modelled using stochastic fields. These are fields (denoted hereafter as $\boldsymbol{\theta}$) that spread a parameter in space with a distribution, which tends to be a Gaussian with an associated mean value μ and standard deviation σ, among correlated points and thus yielding correlated field values. The mathematical definition of correlation ρ_{θ_i,θ_j} is

$$\rho_{\theta_i,\theta_j} = \frac{\mathrm{cov}(\theta_i, \theta_j)}{\sigma_i \sigma_j} = \frac{\mathrm{E}[(\theta_i - \mu_i)(\theta_j - \mu_j)]}{\sigma_i \sigma_j} \tag{5}$$

However, for the sake of convenience of random fields generation, it is more useful to search for an alternative expression for correlation that can be used as input. One of the most common definitions of correlation functions found in literature is the squared exponential, whose expression is:

$$\rho_{\theta_i,\theta_j} = e^{-\left(\frac{\Delta L}{L_c}\right)^2} \tag{6}$$

in which ΔL is the Euclidean distance between the Gauss integration points within each layer and L_c is the correlation distance, which is chosen to be equal to the magnitude d defined in Section 2, as it is the length in which the fibre angle orientation varies along. By employing the squared exponential, a steepest drop in the correlation is found for distances greater than the correlation length as shown in [21].

There is a plethora of methods that can be used for generating stochastic fields [33], presenting each of them its own advantages and disadvantages. Covariance Matrix Decomposition (CMD) method is used hereinafter to generate random fields of fibre misalignments due to its implementation easiness and facility to vary the correlation function and length. The mathematical background of CMD is omitted here, but it can be found in [34].

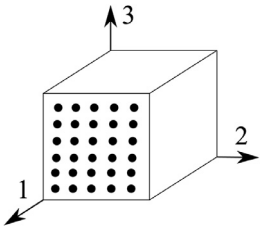

Fig. 3. Material coordinate system. Direction 1 corresponds to the fibre direction while 2 and 3 represent the transverse directions.

4. Failure indices

The Hashin 3D failure criteria and the Mixed mode quadratic criteria are herein used, respectively, for the prognostication of ply failure and the delamination initiation. These failure indices are calculated employing the stress state computed in the material coordinate system, which is depicted in Fig. 3.

The Hashin 3D failure criteria [35] are employed for the determination, based on the stress state, of ply failure and determine the ply level's dominating failure mode. The failure indices for the state of fibre and matrix tension or compression are computed according to the following equations:

1. Fibre tension:

$$\left(\frac{\sigma_{11}}{X_T}\right)^2 + \frac{\sigma_{12}^2 + \sigma_{13}^2}{S_{12}^2} \geq 1 \tag{7}$$

2. Fibre compression

$$\left(\frac{\sigma_{11}}{X_C}\right)^2 \geq 1 \tag{8}$$

3. Matrix tension:

$$\frac{(\sigma_{22} + \sigma_{33})^2}{Y_T^2} + \frac{\sigma_{23}^2 - \sigma_{22}\sigma_{33}}{S_{23}^2} + \frac{\sigma_{12}^2 + \sigma_{13}^2}{S_{12}^2} \geq 1 \tag{9}$$

4. Matrix compression:

$$\left[\left(\frac{Y_C}{2S_{23}}\right)^2 - 1\right]\left(\frac{\sigma_{22} + \sigma_{33}}{Y_C}\right) + \frac{(\sigma_{22} + \sigma_{33})^2}{4S_{23}^2} + \frac{\sigma_{23}^2 - \sigma_{22}\sigma_{33}}{S_{23}^2} + \frac{\sigma_{12}^2 + \sigma_{13}^2}{S_{12}^2} \geq 1 \tag{10}$$

Additionally, delamination index is considered as well, since this failure mechanism has proven to be of major concern when considering manufacturing defects in VAT laminates [36]. The delamination index is calculated by means of the mixed mode quadratic criterion [37], given by the following equation:

$$\left(\frac{\langle\sigma_{33}\rangle}{Z_T}\right)^2+\left(\frac{\sigma_{23}}{S_{23}}\right)^2+\left(\frac{\sigma_{13}}{S_{13}}\right)^2\geq 1 \tag{11}$$

For all the expressions above, σ_{ij} correspond to the stress tensor components computed in the material coordinate system; X and Y represent the material strengths in the fibre and transverse directions respectively and subscripts T and C denote tensile and compressive loading and Z_T is the interlaminar normal strength. Similarly, S_{ij} represents the material shear strengths. Finally, $\langle\sigma_{33}\rangle$ in Eq. (11) denotes $max(0,\sigma_{33})$, being σ_{33} the transverse normal stress.

The accurate evaluation of failure indices employing high-order 1D models is supported by the outcomes of the study conducted by de Miguel et al. [38], where the same criteria were used to determine the mode of failure initiation and the the loads at which first ply failure occurs. The 1D models showed a 10 to 20 times reduction in the number of degrees of freedom than 3D models, which meant a one to twofold reduction in the CPU time.

5. Layerwise approach applied to VAT panels

5.1. Carrera unified formulation

In this work, VAT composite laminates are modelled exploiting refined 1D CUF models, which have been proven to deliver precise results for a wide variety of structural geometries and material anisotropy, see [39]. Under the scope of CUF, the three dimensional displacement field can be expressed in terms of an arbitrary cross-section expansion, $F_\tau(x,z)$, of the 1D generalised unknowns laying along the longitudinal direction which is coincident with the y-axis, that is:

$$\mathbf{u}(x,y,z)=F_\tau(x,z)\mathbf{u}_\tau(y)\quad \tau=1,\dots,M \tag{12}$$

in which M is the number of expansion terms and $\mathbf{u}_\tau(y)$ is the vector of the generalised displacements. The selection of $F_\tau(x,z)$ and M can be opportunely made depending on the demanded accuracy. Different expansions have been used in the analysis of laminated structures such as Taylor (TE), Lagrange (LE) and Hierarchical Legendre (HLE) expansions that the reader can find in the work by Pagani et al. [39].

5.2. Finite element approximation

The finite element (FE) formulation has been chosen in this work because of the advantages demonstrated in the analysis of diverse geometries and boundary conditions. Consequently, the generalised displacements are described as functions of the unknown nodal vector $\mathbf{u}_{\tau i}$ and the shape functions $N_i(y)$ as:

$$\mathbf{u}_\tau(y)=N_i(y)\mathbf{u}_{\tau i}\quad i=1,\dots,n_{elem} \tag{13}$$

where n_{elem} is the number of nodes per element. In the present work, Lagrange interpolation polynomials have been employed to define FEs. However, a plethora of sets can be used for such purpose. For the sake of brevity, these expressions are not reported herein but they are available in the book by Carrera et al. [40], where linear (B2), quadratic (B3) and cubic (B4) beam elements are depicted. Finally, introducing Eq. (13) into Eq. (12), yields the expression for the displacement field as:

$$\mathbf{u}(x,y,z)=F_\tau(x,z)N_i(y)\mathbf{u}_{\tau i}\quad \tau=1,\dots,M\quad i=1,\dots,n_{elem} \tag{14}$$

Once the structural theory and the approximation resolution method is introduced, the principle of virtual displacements (PVD) is employed to derive the expression for the FE governing equations. PVD states that:

$$\delta L_{int}=\delta L_{ext} \tag{15}$$

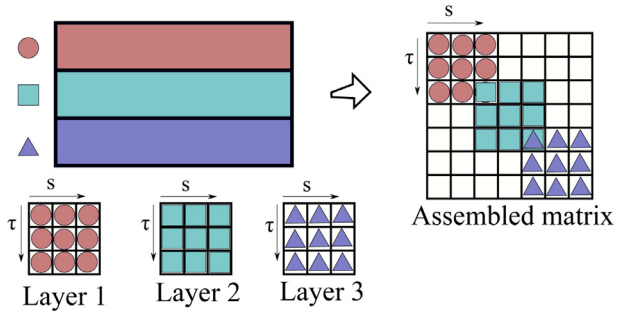

Fig. 4. Assembly of the stiffness matrix using a layerwise approach.

Table 1
Material properties of the two-layered plate used in [27] and material strength values used to compute delamination and failure indices.

Material properties		Strength characteristics	
E_1 [GPa]	137.9	Z_T [MPa]	60.0
E_2, E_3 [GPa]	8.96	S_{13} [MPa]	174.54
G_{12}, G_{13} [GPa]	8.96	S_{23} [MPa]	152.66
G_{23} [GPa]	6.21	X_T [MPa]	2586.0
ν_{12}, ν_{13}	0.30	Y_T [MPa]	94.0
ν_{23}	0.49	S_{23} [MPa]	174.54

where δL_{int} is the virtual variation of the internal strain energy

$$\delta L_{int}=\int_V \delta\boldsymbol{\varepsilon}^T\boldsymbol{\sigma} \tag{16}$$

and δL_{ext} is the virtual work due to external loadings

$$\delta L_{ext}=F_s N_j \delta\mathbf{u}_{sj}^T\mathbf{P} \tag{17}$$

in which $\mathbf{P}$ is the vector of the applied point load components (3×1).

δL_{int} can be formulated using Eqs. (14) and (16), the constitutive law (Eq. (3)) and the geometrical relations which results in the following equation for the stiffness matrix:

$$\delta L_{int}=\delta\mathbf{u}_{sj}\mathbf{K}^{ij\tau s}\mathbf{u}_{\tau i} \tag{18}$$

in which $\mathbf{K}^{ij\tau s}$ is the 3×3 fundamental nucleus (FN), which is independent of the order of the 1D model and the expansion for the cross-section, see for instance the CUF book [40]. The mathematical expression for FN results in:

$$\mathbf{K}^{ij\tau s}=\int_V \mathbf{D}^T(N_i F_\tau)\tilde{\mathbf{C}}\mathbf{D}(N_j F_s)dV \tag{19}$$

in which $\mathbf{D}$ is the differential operator containing the geometrical relations between strains and displacements and $\tilde{\mathbf{C}}$ is the material stiffness matrix from Eq. (4). Conversely from other CUF-based works, Eq. (19) can not be split into separate integrals where the FE solution and CUF expansion are independently evaluated, and therefore a 3D integration is needed. Finally, the global assembled stiffness matrix $\tilde{\mathbf{K}}$ is obtained by looping through the indices i,j,τ,s.

5.3. Layerwise models

When it comes to the analysis of laminated structures, two valid approaches arise: Equivalent single layer (ESL) and Layerwise (LW) approaches. Because of the outcomes of previous works considering manufacturing flaws at the mesoscale level of composite structures [22], LW approach is considered mandatory for such analysis and, therefore, it is the methodology chosen in the present work. By using LW strategy, the contribution of each layer to the structure's stiffness matrix is considered individually and, then, the correspondence of the shared-sides of the cross-section expansion domains guarantees the continuity of the displacement solutions, i.e.:

$$\mathbf{u}_{top}^k=\mathbf{u}_{bottom}^{k+1} \tag{20}$$

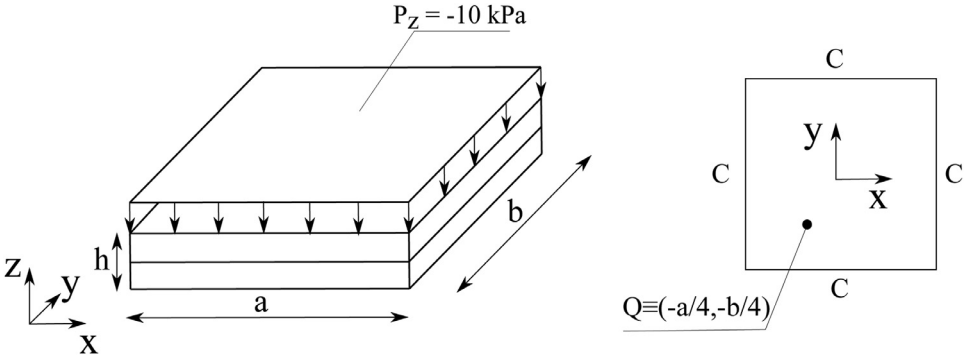

Fig. 5. Boundary conditions of the two-layered plate by [27]. C stands for clamped edge and Q corresponds to the point where displacements, stresses and failure indices are calculated at.

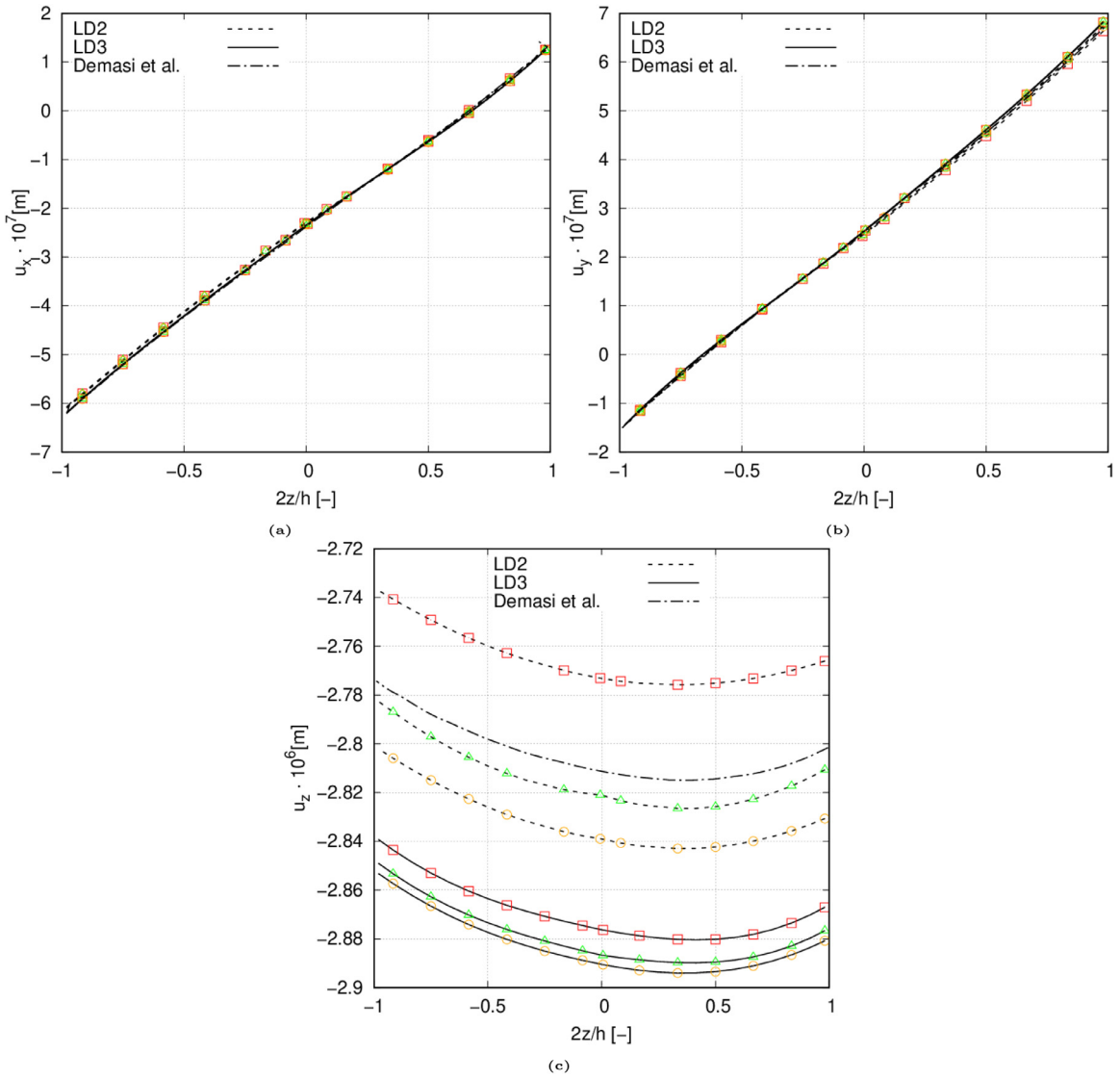

Fig. 6. Through-the-thickness displacement field, measured at point Q, for the different number mesh elements and element theory. 6×6 mesh □, 8×8 mesh △, 10×10 mesh ∘. LD2 and LD3 stand for quadratic and cubic element order. The $[< 90, 45 >, < 0, 45 >]$ plate is clamped in its four edges and a constant pressure $Pz = -10$ kPa is exerted at $z = h/2$.

where the superscript k accounts for the layer numbering. For practical reasons, in this manuscript the LW approach is obtained by means of LE polynomials. In this work nine-node and sixteen-node polynomials are employed. These polynomials provide, respectively, quadratic and cubic expansion models which are known in the literature as LD2 and LD3, see the book by Carrera et al. [40]. Note that the letter L stands for "layerwise", whereas D is for "displacement" as opposed to M, which means "mixed" refined models as described in the mentioned work. For the sake of completeness, the displacement field of an LD3 model is given in the following:

$$u_x = F_1(x,z)u_{1x} + F_2(x,z)u_{2x} + F_3(x,z)u_{3x} + F_4(x,z)u_{4x} + ... + F_{16}(x,z)u_{16x}$$

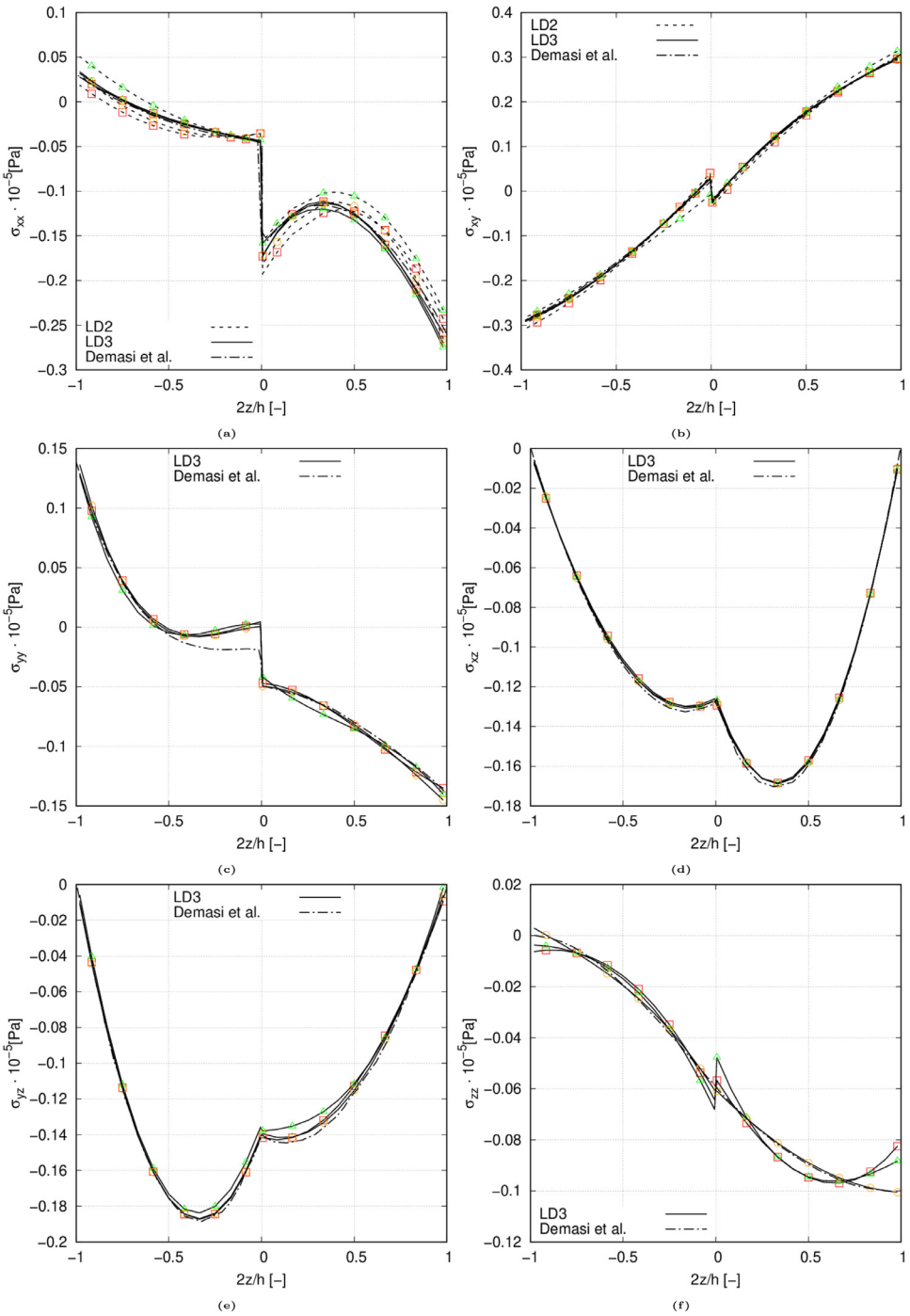

Fig. 7. Through-the-thickness stress field, measured at point Q, for the different number mesh elements and element theory. 6×6 mesh □, 8×8 mesh △, 10×10 mesh ∘. LD2 and LD3 stand for quadratic and cubic element order. The $[<90,45>,<0,45>]$ plate is clamped in its four edges and a constant pressure $Pz = -10$ kPa is exerted at $z = h/2$.

$$
\begin{aligned}
u_y &= F_1(x,z)u_{1y} + F_2(x,z)u_{2y} + F_3(x,z)u_{3y} + F_4(x,z)u_{4y} + ... + F_{16}(x,z)u_{16y} \\
u_z &= F_1(x,z)u_{1z} + F_2(x,z)u_{2z} + F_3(x,z)u_{3z} + F_4(x,z)u_{4z} + ... + F_{16}(x,z)u_{16z}
\end{aligned} \tag{21}
$$

The different terms of $F_\tau(x,z)$ for the LD3 expansion included in Eqs. (21) can be found by the reader in the work by Carrera and Petrolo [41]. Note that by the usage of LE polynomials, condition (20) is automatically fulfilled since the degrees of freedom of the resulting models coincide with pure displacements. Such condition can be reached as well employing TE polynomials and giving special consideration to the interface conditions [42,43]. Finally, the assembling of the stiffness matrix of a laminated structure exploiting the LW approach can be appreciated in Fig. 4.

6. Results

6.1. Validation

The most refined layerwise results presented by Demasi et al. [27] are used for validation of the CUF-based LW-models employed in this manuscript. The model used in the mentioned reference consists of a plate composed by two layers. The plate has width and length $a = b = 1$ m and a total thickness $h = 0.1$ m. The material properties are shown in Table 1. The plate is clamped in all four edges and loaded with a constant pressure $P_z = -10$ kPa applied on the top surface. The displacements and stresses are computed at point $Q \equiv (-a/4, -b/4)$, see Fig. 5. Finally, the fibre angle orientations for the first and second layer are

Table 2
Convergence of the displacement field evaluated at $2z/h = 0.4160$ for the $[< 90, 45 >, < 0, 45 >]$ plate studied in [27].

Model	Mesh	DOF	$u_x \cdot 10^7$ [m]	$u_y \cdot 10^7$ [m]	$u_z \cdot 10^6$ [m]
Demasi et al. [27]	-	391040	0.9251	4.208	2.814
LD3	10×10	20181	0.9256	4.258	2.894
	8×8	13125	0.9250	4.252	2.890
	6×6	7581	0.9193	4.245	2.880
LD2	10×10	6615	0.9276	4.186	2.843
	8×8	4335	0.9241	4.174	2.826
	6×6	2535	0.9028	4.125	2.776
LD1	10×10	2640	0.6506	3.473	2.208
	8×8	1728	0.6834	3.432	2.104
	6×6	1008	0.4111	2.554	1.669

Table 3
Convergence of the stress field evaluated at $2z/h = 0.4160$ for the $[< 90, 45 >, < 0, 45 >]$ plate studied in [27].

Model	Mesh	$\sigma_{xx} \cdot 10^{-5}$ [Pa]	$\sigma_{yy} \cdot 10^{-5}$ [Pa]	$\sigma_{zz} \cdot 10^{-5}$ [Pa]	$\sigma_{xz} \cdot 10^{-5}$ [Pa]	$\sigma_{yz} \cdot 10^{-5}$ [Pa]	$\sigma_{xy} \cdot 10^{-5}$ [Pa]
Demasi et al. [27]	-	0.1191	0.0714	0.0859	0.1679	0.1284	0.1462
LD3	10×10	0.1158	0.0729	0.0853	0.1661	0.1256	0.1505
	8×8	0.1235	0.0793	0.0915	0.1663	0.1205	0.1487
	6×6	0.1153	0.0740	0.0914	0.1654	0.1235	0.1511
LD2	10×10	0.1122	0.0652	0.0792	0.1353	0.1073	0.1470
	8×8	0.1011	0.0763	0.0834	0.1318	0.1444	0.1515
	6×6	0.1208	0.0619	0.0765	0.1312	0.0985	0.1404
LD1	10×10	0.1301	0.0569	0.0643	0.1196	0.1108	0.0993
	8×8	0.0754	0.0814	0.0169	0.0101	0.1679	0.1227
	6×6	0.1116	0.0648	0.1211	0.1145	0.0984	0.0829

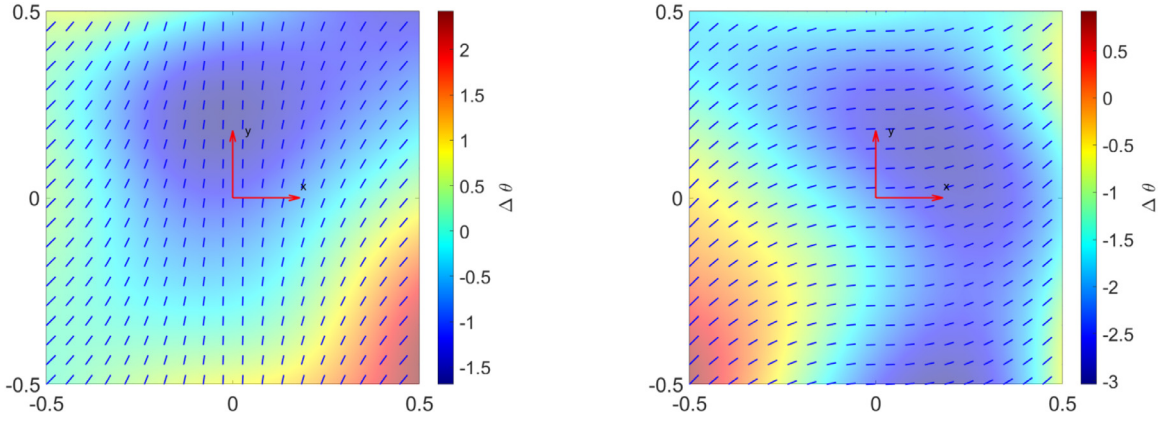

(a) Random field on a $[< 90, 45 >]$ ply. (b) Random field on a $[< 0, 45 >]$ ply.

Fig. 8. Example of two randomly distributed fibre misalignment with zero mean and standard deviation of $\sigma_\theta = 1.5°$ applied on $[< 90, 45 >]$ and $[< 0, 45 >]$ plies.

respectively $< T_0^1, T_1^1 >=< 90, 45 >$ and $< T_0^2, T_1^2 >=< 0, 45 >$ in the notation depicted previously.

A mesh convergence analysis in which the number of elements along the x and y-axes are varied along with the element order, that is, quadratic (LD2/B3) and cubic (LD3/B4), is carried out. Figs. 6 and 7 show respectively the displacement and stresses field at point Q obtained with the different combinations of element order and number of elements. In Fig. 6 it can be appreciated that a 6×6 mesh using second order elements are sufficient to obtain u_x and u_y variation, while for u_z distribution a 8×8 mesh using LD2 provide accurately enough results. For the through-the-thickness variation of the u_z a small relative difference of about 3% is found with respect to Demasi's work, although a refined mesh and LD3 expansion is used. However, it is worth noting that this 3% difference is obtained by employing, approximately, just a 5% of the degrees of freedom (DOF) from Demasi's model (reported in Table 2). As far as the stress distributions are concerned, note that the LD2 model is only given for the σ_{xx} and σ_{xy} in Figs. 7(a) and 7(b) as it gives inconsistent results for the remaining components. For all the stress components it is clear from Fig. 7 that the LD3 model is fully compliant with the reference results and the elasticity C_0^z equilibrium/compatibility conditions. It is demonstrated indeed that the 8×8 and 10×10 LD3 meshes provide the greatest accuracy, excluding σ_{zz} distribution where the latter outperforms the former by providing the exact reference results, which can be better perceived in Table 3. Thus, the 10×10 LD3 mesh is the one chosen for the following computational analyses.

6.2. *Influence of fibre misalignments on stress distribution and failure indices*

The influence of fibre misalignments on the stress distribution and failure indices of the previous plate is analysed. The CMD method commented in Section 3 is employed to generate the misalignment field of the fibre path of each lamina. These fields are obtained by means of the same correlation matrix **R**, since the relative distances only depend on the in-plane coordinates of the ply. In these numerical results, a fi-

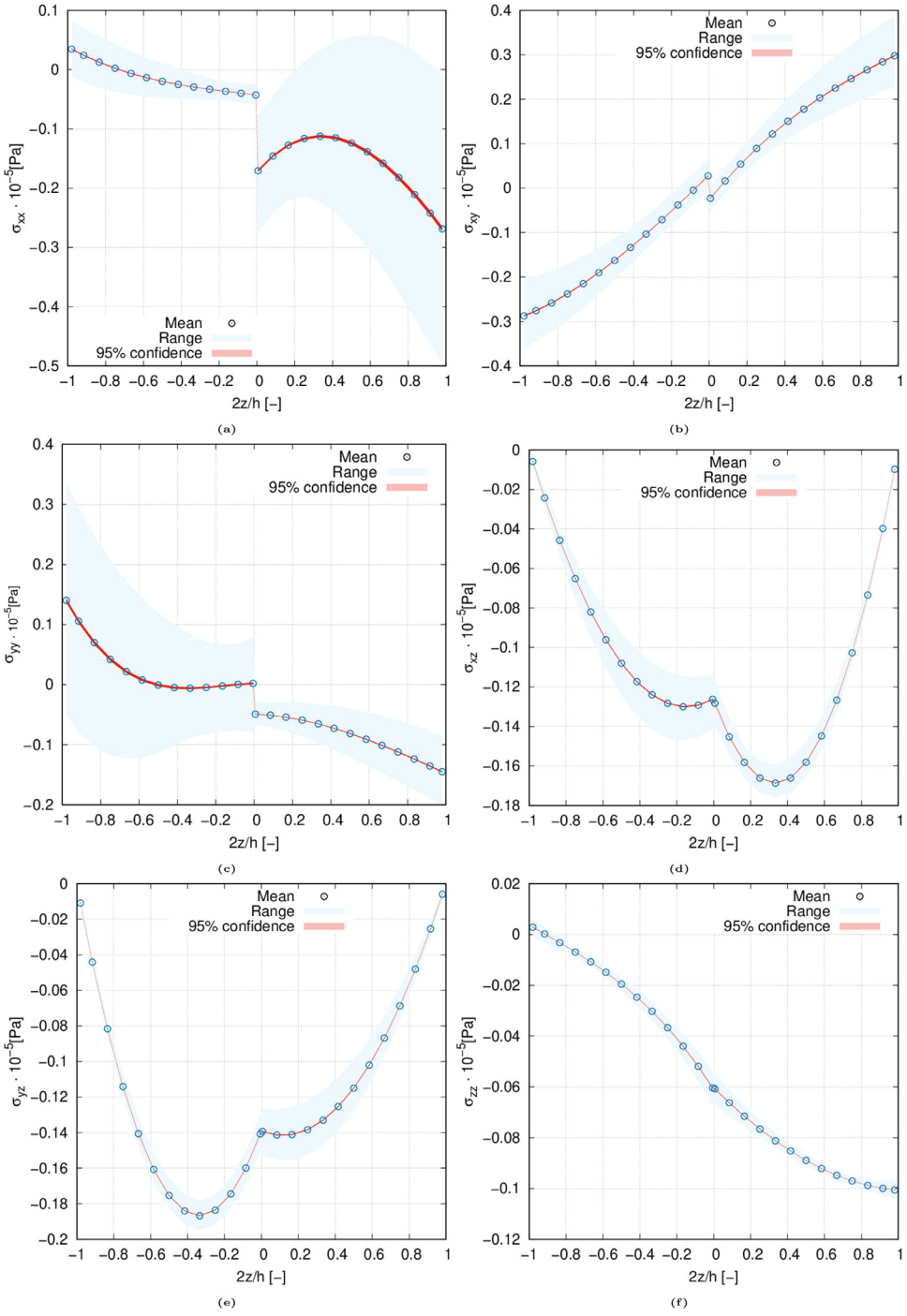

Fig. 9. Through-the-thickness stress field, measured at point Q, for the pristine and flawed structure. The $[<90,45>,<0,45>]$ plate is clamped in its four edges and a constant pressure $Pz = -10$ kPa is exerted at $z = h/2$. Mean value, range and 95% confidence interval are displayed. The fibre misalignment field has a null mean and standard deviation equal to $\sigma_\theta = 1.5°$.

bre misalignment stochastic field with null mean and standard deviation equal to $\sigma_\theta = 1.5°$ is generated. This is supposed to be a reasonable value in both classical and tow-steered composites, see [10–13]. Examples of such misalignments fields with the aforementioned statistical properties applied to $[<90,45>]$ and $[<0,45>]$ fibre paths are shown in Fig. 8.

A thousand Monte Carlo simulations are carried out and through-the-thickness stresses are computed again at point Q for the flawed structure. The outcomes of the simulations are shown in Fig. 9. These plots represent the mean values, maximum-minimum range and 95% confidence interval of each magnitude. It can be appreciated in Tables 3 and 4 that the mean value of the stresses barely differ from those presented by the pristine structure. Additionally, as opposed to the maximum-minimum range, the 95% confidence intervals do not present an exacerbated variation of the stress distribution. Note that the range intervals of σ_{xx} and σ_{yy} are large and variation of the stress component for the same nondimensional coordinate may occur. This variability might lead to undesired effects and lately affect failure indices. Stresses in the local fibre direction are represented in Fig. 10 as well for a better comprehension of the failure index distributions later on.

Regarding failure indices, results for Hashin 3D criterion are appreciated in Fig. 11. Values of the material strengths involved in both criteria are listed in Table 1. Fibre failure is analysed in the first instance since its main component (σ_{11}) shows in Fig. 10(a) a great sign variability throughout the realisations. However, two intervals along the dimensionless thickness coordinate ($2z/h \in [-0.66, -0.40] \cup [0, 0.10]$) only present compression stresses, and therefore failure due to fibre compres-

Table 4
Statistics of the stress field evaluated at $2z/h = 0.4160$ for the $[<90,45>,<0,45>]$ plate studied in [27] after performing the Monte Carlo analysis.

	$\sigma_{xx} \cdot 10^{-5}$ [Pa]	$\sigma_{yy} \cdot 10^{-5}$ [Pa]	$\sigma_{zz} \cdot 10^{-5}$ [Pa]	$\sigma_{xz} \cdot 10^{-5}$ [Pa]	$\sigma_{yz} \cdot 10^{-5}$ [Pa]	$\sigma_{xy} \cdot 10^{-5}$ [Pa]
Mean value	0.1151	0.0727	0.0854	0.1661	0.1254	0.1507
Standard deviation	0.0368	0.0085	0.0007	0.0023	0.0037	0.0118
Minimum-Maximum Range	[0.2421,0.04714]	[0.10763,0.03586]	[0.08529,0.08521]	[0.1735,0.1559]	[0.1386,0.1089]	[0.1120,0.2024]
95% C.I.	[0.1174,0.1128]	[0.07324,0.07219]	[0.08763,0.08258]	[0.1662,0.1659]	[0.1256,0.1252]	[0.1499,0.1514]

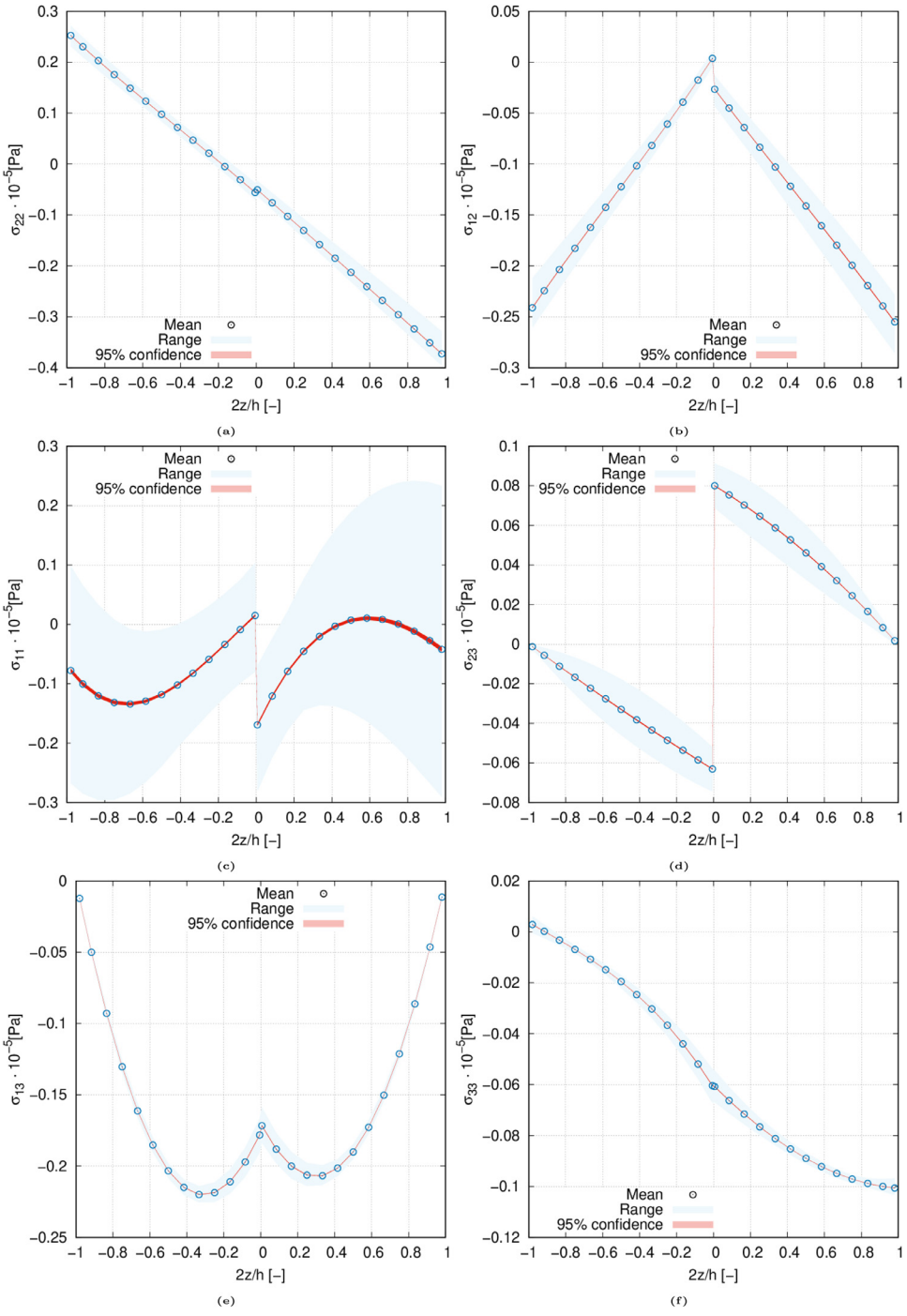

Fig. 10. Through-the-thickness local stress field, measured at point Q, for the pristine and flawed structure. The $[<90,45>,<0,45>]$ plate is clamped in its four edges and a constant pressure $Pz = -10$ kPa is exerted at $z = h/2$. Mean value, range and 95% confidence interval are displayed. The fibre misalignment field has a null mean and standard deviation equal to $\sigma_\theta = 1.5°$.

sion is the only failure mechanism involving fibres in such intervals. For a better understanding of the σ_{11} variability, probability density functions (PDFs) are represented in Fig. 12. From this plot it can be inferred that the lower lamina is mainly subjected to a compressive state in the different realisations when fibre misalignments are considered. The upper part is mainly subjected to compressive stresses as well, although tensional stresses are obtained too. These σ_{11} tensional components correspond to outlier values, which are not within the 95% confidence interval, and provide the results displayed in Fig. 11(a) where σ_{12} and σ_{13} are considered too, according to Eq. (7).

For the case of matrix failure (Figs. 11(c) and 11(d)) it can be appreciated that the structure would be prone to fail because of matrix

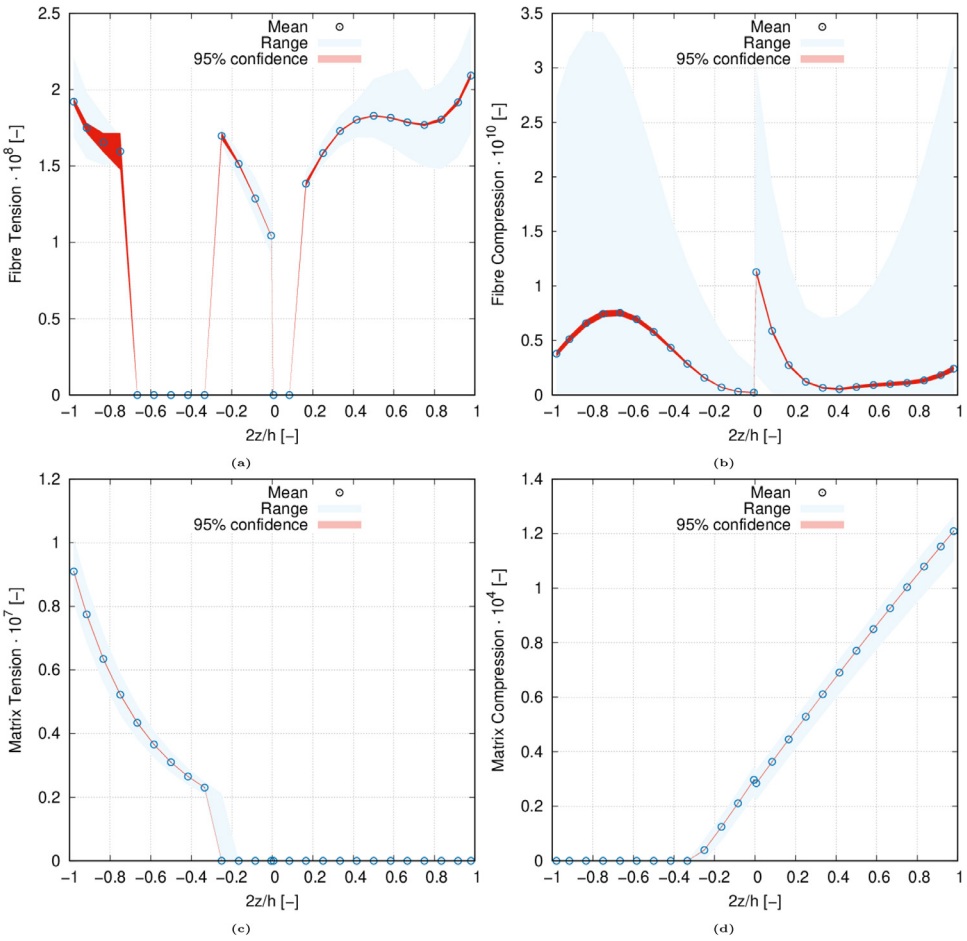

Fig. 11. Through-the-thickness failure index based on Hashin 3D, measured at point Q, for the pristine and flawed structure. The $[<90,45>,<0,45>]$ plate is clamped in its four edges and a constant pressure $Pz = -10$ kPa is exerted at $z = h/2$. Mean value, range and 95% confidence interval are displayed. The fibre misalignment field has a null mean and standard deviation equal to $\sigma_\theta = 1.5°$.

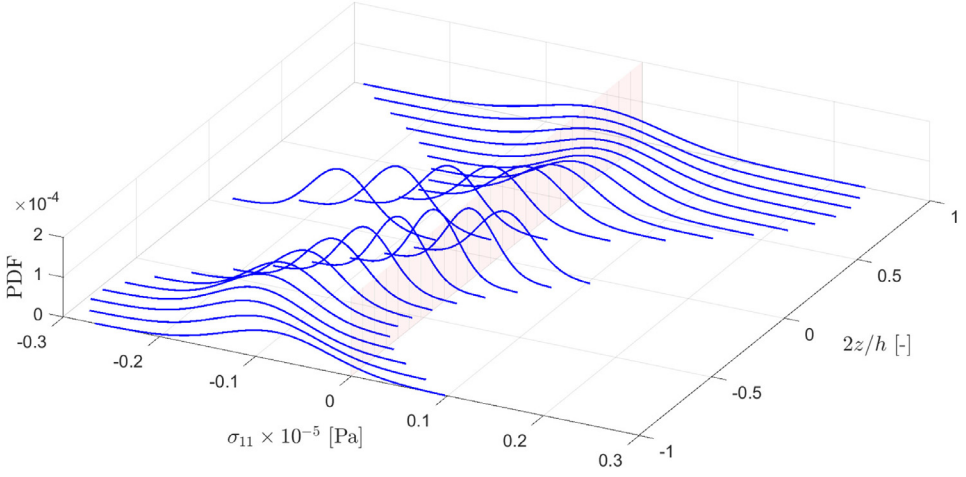

Fig. 12. Through-the-thickness PDFs of the local stress σ_{11}, computed at point Q, in the material reference. The divisory plane represents the change in tension-compression stress state. The $[<90,45>,<0,45>]$ plate is clamped in its four edges and a constant pressure $Pz = -10$ kPa is exerted at $z = h/2$. The fibre misalignment field has a null mean and standard deviation equal to $\sigma_\theta = 1.5°$.

compression rather than matrix tension. Moreover, this failure might occur within the upper layer of the laminate. This differentiation is due to the local stress distributions regarding σ_{22} and σ_{33} (see Figs. 10(c) and 10(d)), where the former is one order of magnitude larger and therefore dominating in the sum of both, which determines whether the matrix is under a tension ($\sigma_{22} + \sigma_{33} > 0$) or compression state. Note that, contrarily to fibre failure, there is an obvious failure mode differentiation between the two layers conforming the laminate.

Delamination index is plotted in Fig. 13 where it shows a narrow confidence interval along with a relatively small range. This range happens to be wider in the vicinity of the plies interface. Great shape similarity can be appreciated between Fig. 10(e) and delamination index, which is due to the compressional behaviour of σ_{33}, which does not take part in Eq. (11).

Finally, the aforementioned statistical properties of the considered failure indices, computed at $2z/h = 0.4160$, are listed in Table 5. Because of the null value of matrix tension in that point, such statistical properties are evaluated at $2z/h = -0.4160$. In this table it is appreciated the small variability, in terms of the 95% confidence interval, of the failure indices when misalignments are taken into account. A wide variation is, however, found for the case of fibre failure because of the vast variations that the in-plane stresses presented beforehand. It is worth reminding

Table 5
Statistics of the failure indices evaluated at $2z/h = 0.4160$ for the $[<90,45>,<0,45>]$ plate studied in [27] after performing the Monte Carlo analysis. The plate was subjected to a constant pressure $P_z = -10$kPa at $z = h/2$. (*) Results regarding Matrix Tension are computed at $2z/h = -0.4160$.

	Fibre Tension·10^8	Fibre Compression·10^{10}	Matrix Tension·10^7 (*)	Matrix Compression·10^4	Delamination ·10^8
Mean value	1.80	0.055	0.265	0.6902	1.451
Standard deviation	0.04	0.10	0.081	0.0123	0.031
Minimum-Maximum Range	[1.69,1.93]	[0,0.72]	[0.239,0.291]	[0.6124,0.7391]	[1.329,1.529]
95% C.I.	[1.79,1.81]	[0.046,0.063]	[0.265,0.266]	[0.6894,0.6909]	[1.448,1.453]

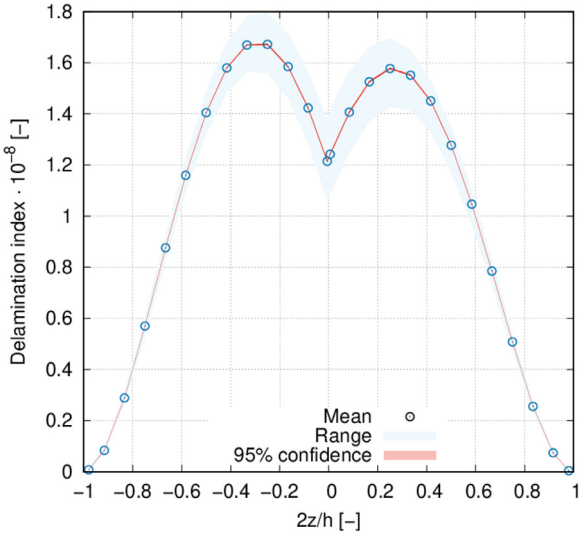

Fig. 13. Through-the-thickness delamination index based on mixed mode quadratic criterion, computed at point Q, in the material reference frame for the pristine and flawed structure. The $[<90,45>,<0,45>]$ plate is clamped in its four edges and a constant pressure $Pz = -10$ kPa is exerted at $z = h/2$. The fibre misalignment field has a null mean and standard deviation equal to $\sigma_\theta = 1.5°$.

that these failure indices are computed for a linear static analysis, which means that if a different load magnitude was imposed these results will vary proportionally.

7. Conclusions

In this work, a one dimensional model based on the Carrera Unified Formulation (CUF) has been employed for the linear static and stochastic failure analysis of VAT composites. For the purpose of this study, a VAT plate introduced by Demasi et al. [27] has been used as a reference for validation purposes. A mesh convergence analysis was performed in order to find the mesh that presents the best trade off between accuracy and computational effort. Results showed the best accuracy when cubic elements are employed for either finite elements (B4) and cross-section (L16) expansion along the y-axis and the $x-z$ plane respectively, thus obtaining a high-order layerwise (LW) description of the model unknowns.

The influence of fibre misalignments on the stress and failure index distribution has been subsequently characterised by means of Monte Carlo analyses. Such fibre misalignments have been modelled as a normal distribution of null mean and 1.5 degrees standard deviation and spread within the laminate using stochastic fields computed by means of the Covariance Matrix Decomposition (CMD) method. Results showed a large variability for the case of in-plane stresses σ_{xx} and σ_{yy}, whilst σ_{xy} and the out-of-plane stresses did not present such large variations. Then, these stress outcomes have been used for the computation of Hashin 3D and Mixed mode delamination failure indices in the material coordinate reference frame. Hashin 3D comprises fibre and matrix failure. The latter displayed a very differentiated behaviour through the thickness of the laminate, being it more prone to fail because of matrix compression in the upper layer while the bottom one is subjected to matrix tension. Regarding delamination distribution, it is mainly dominated by the shear stresses ever since the normal stress does not contribute to the delamination onset because of its compressive character.

As a general comment, the stochastic analysis has demonstrated that the delamination strength of VAT composite structures is less affected by fibre misalignment if compared to other failure mechanisms. Although one single plate layout is described in this work for the sake of conciseness, other analyses have confirmed that this latter remark applies also to other VAT configurations.

Future work will deal with multi-scale stochastic analysis of variable stiffness composites for the characterization of the effect of manufacturing defects, possibly in a nonlinear framework.

Acknowledgments

This project has received funding from the European Research Council (ERC) under the European Unions Horizon 2020 research and innovation programme (Grant agreement no. 850437).

References

[1] Z. Gürdal, R. Olmedo, In-plane response of laminates with spatially varying fiber orientations - variable stiffness concept, AIAA J. 31 (4) (1993) 751–758.
[2] Z. Gürdal, R. Olmedo, Buckling response of laminates with spatially varying fiber orientations, in: Proceedings of the 34th Structures, Structural Dynamics and Materials Conference, AIAA, La Jolla, California, USA, 1993.
[3] F. Heinecke, C. Willberg, Manufacturing-induced imperfections in composite parts manufactured via automated fiber placement, J. Compos. Sci. 3 (2) (2019) 56.
[4] A.W. Blom, C.S. Lopes, P.J. Kromwijk, Z. Gurdal, P.P. Camanho, A theoretical model to study the influence of tow-drop areas on the stiffness and strength of variable-stiffness laminates, J. Compos. Mater. 43 (5) (2009) 403–425.
[5] K. Fayazbakhsh, M.A. Nik, D. Pasini, L. Lessard, Defect layer method to capture effect of gaps and overlaps in variable stiffness laminates made by automated fiber placement, Compos. Struct. 97 (2013) 245–251.
[6] M.A. Nik, K.K. Fayazbakhsh, D. Pasini, L. Lessard, Optimization of variable stiffness composites with embedded defects induced by automated fiber placement, Compos. Struct. 107 (2014) 160–166.
[7] C.S. Lopes, Damage and failure of non-conventional composite laminates, Delft University of Technology, 2009. PhD thesis
[8] D.H.J.A. Lukaszewicz, C. Ward, K.D. Potter, The engineering aspects of automated prepreg layup: History, present and future, Compos. Part B: Eng. 43 (3) (2012) 997–1009.
[9] K. Voltzer, Online-Prozessüberwachung von Automated Fiber Placement Prozessen auf Basis der Thermografie, Gottfried Wilhelm Leibniz Universitt Hannover, 2018. PhD thesis
[10] K. Potter, B. Khan, M. Wisnom, T. Bell, J. Stevens, Variability, fibre waviness and misalignment in the determination of the properties of composite materials and structures, Compos. Part A: Appl. Sci. Manuf. 39 (9) (2008) 1343–1354.
[11] M.R. Wisnom, The effect of fibre misalignment on the compressive strength of unidirectional carbon fibre/epoxy, Composites 21 (5) (1990) 403–407.
[12] B.A. Bednarcyk, J. Aboudi, S.M. Arnold, The effect of general statistical fiber misalignment on predicted damage initiation in composites, Compos. Part B: Eng. 66 (2014) 97–108.
[13] T.S. Mesogitis, A.A. Skordos, A.C. Long, Stochastic simulation of the influence of fibre path variability on the formation of residual stress and shape distortion, Polym. Compos. 38 (12) (2017) 2642–2652.
[14] H.C. Mateus, C.M.M. Soares, C.A.M. Soares, Sensitivity analysis and optimal design of thin laminates composite structures, Comput. Struct. 41 (3) (1991) 501–508.
[15] I.M. Sobol, Global sensitivity indices for nonlinear mathematical models and their Monte Carlo estimates, Math. Comput. Simul. 55 (1) (2001) 271–280.
[16] C.A.C.a. António, L.N. Hoffbauer, Uncertainty assessment approach for composite structures based on global sensitivity indices, Compos. Struct. 99 (2013) 202–212.

[17] S. Dey, T. Mukhopadhyay, S. Adhikari, Stochastic free vibration analysis of angle-ply composite plates: a RS-HDMR approach, Compos. Struct. 122 (2015) 526–536.
[18] M. Thapa, A. Paudel, S.B. Mulani, R.W. Walters, Global sensitivity analysis for stochastic responses of fiber reinforced composites with polynomial chaos, in: Proceedings of the AIAA Scitech 2020 Forum, Orlando, Florida, USA, 2020, pp. 6–10.
[19] C. Scarth, S. Adhikari, P. Cabral, G. Silva, A. Prado, Random field simulation over curved surfaces: applications to computational structural mechanics, Comput. Methods Appl. Mech. Eng. 345 (2019) 283–301.
[20] S. van den Broek, S. Minera, A. Pirrera, P. Weaver, E. Jansen, R. Rolfes, Enhanced deterministic performance of panels using stochastic variations of geometric and material parameters, in: Proceedings of the AIAA Scitech 2019 Forum, San Diego, California, USA, 2019, pp. 7–11.
[21] S. van den Broek, S. Minera, E. Jansen, A. Pirrera, P. Weaver, R. Rolfes, Improving the static structural performance of panels with spatially varying material properties using correlations, in: M. Petrolo (Ed.), Advances in Predictive Models and Methodologies for Numerically Efficient Linear and Nonlinear Analysis of Composites, Springer International Publishing, Cham, 2019, pp. 143–158.
[22] A. Pagani, A.R. Sanchez-Majano, Influence of fiber misalignments on buckling performance of variable stiffness composites using layerwise models and random fields, Mech. Adv. Mater. Struct. (2020) 1–15, Paper in press, doi:10.1080/15376494.2020.1771485.
[23] E. Carrera, Theories and finite elements for multilayered plates and shells: a unified compact formulation with numerical assessment and benchmarking, Arch. Comput. Methods Eng. 10 (2003) 215–296.
[24] E. Carrera, A. Pagani, M. Petrolo, E. Zappino, Recent developments on refined theories for beams with applications, Mech. Eng. Rev. 2 (2) (2015) 14-00298.
[25] R. Vescovini, L. Dozio, A variable-kinematic model for variable stiffness plates: vibration and buckling analysis, Compos. Struct. 142 (2016) 15–26.
[26] R. Vescovini, E. Spigarolo, E.L. Jansen, L. Dozio, Efficient post-buckling analysis of variable-stiffness plates using a perturbation approach, Thin-Wall. Struct. 143 (2019) 106211.
[27] L. Demasi, G. Biagini, F. Vannucci, E. Santarpia, R. Cavallaro, Equivalent single layer, zig-zag, and layer wise theories for variable angle tow composites based on the generalized unified formulation, Compos. Struct. 177 (2017) 54–79.
[28] L. Demasi, G. Biagini, F. Vannucci, E. Santarpia, R. Cavallaro, Generalized unified formulation - based bending analysis of variable angle tow panels in the presence of hole, in: Proceedings of the 2018 AIAA/ASCE/AHS/ASC Structures, Structural Dynamics, and Materials Conference, AIAA, 2018.
[29] A. Viglietti, E. Zappino, E. Carrera, Analysis of variable angle tow composites structures using variable kinematic models, Compos. Part B: Eng. 171 (2019) 272–283.
[30] A. Viglietti, E. Zappino, E. Carrera, Free vibration analysis of variable angle-tow composite wing structures, Aerosp. Sci. Technol. 92 (2019) 114–125.
[31] A. Alhajahmad, M.M. Abdalla, Z. Gürdal, Design tailoring for pressure pillowing using tow-placed steered fibers, J. Aircr. 45 (2) (2008) 630–640.
[32] J.N. Reddy, Mechanics of Laminated Composite Plates and Shells: Theory and Analysis, CRC Press, Boca Raton, Florida, USA, 2004.
[33] P.D. Spanos, B.A. Zeldin, Monte Carlo treatment of random fields: a broad perspective, Appl. Mech. Rev. 51 (3) (1998) 219–237.
[34] M.W. Davis, Production of conditional simulations via the lu triangular decomposition of the covariance matrix, Math. Geol. 19 (1987) 91–98.
[35] Z. Hashin, Failure criteria for unidirectional fiber composites, J. Appl. Mech. 47 (2) (1980) 329–334.
[36] O. Falcó, J.A. Mayugo, C.S. Lopes, N. Gascons, J. Costa, Variable-stiffness composite panels: defect tolerance under in-plane tensile loading, Compos. Part A: Appl. Sci. Manuf. 63 (2014) 21–31.
[37] J.C. Brewer, P.A. Lagace, Quadratic stress criterion for initiation of delamination, J. Compos. Mater. 22 (12) (1988) 1141–1155.
[38] A.G. de Miguel, I. Kaleel, M.H. Nagaraj, A. Pagani, M. Petrolo, E. Carrera, Accurate evaluation of failure indices of composite layered structures via various FE models, Compos. Sci. Technol. 167 (2018) 174–189.
[39] A. Pagani, A.G. de Miguel, M. Petrolo, E. Carrera, Analysis of laminated beams via unified formulation and Legendre polynomial expansions, Compos. Struct. 156 (2016) 78–92.
[40] E. Carrera, M. Cinefra, M. Petrolo, E. Zappino, Finite Element Analysis of Structures through Unified Formulation, Wiley & Sons, Hoboken, New Jersey, USA, 2014.
[41] E. Carrera, M. Petrolo, Refined beam elements with only displacement variables and plate/shell capabilities, Meccanica 47 (3) (2012) 537–556.
[42] E. Carrera, A. Pagani, M. Petrolo, Use of Lagrange multipliers to combine 1D variable kinematic finite elements, Comput. Struct. 129 (2013) 194–206.
[43] E. Carrera, A. Pagani, Multi-line enhanced beam model for the analysis of laminated composite structures, Compos. Part B: Eng. 57 (2014) 112–119.